Experimental Investigations on Weld Bead Geometry and Process Optimization in Robot Assisted Wire Arc Additive Manufacturing

Sachin Alawe[1], Prof. Ghanshyam Dhanera[2], Prof. Radheshyam chherkee[3]
[1]*M.E. Scholar Department of Mechanical Engineering, BM College of Technology, Indore (M.P.) India*
[2]*Assistant Professor Department of Mechanical Engineering, BM College of Technology, Indore (M.P.) India*
[3]*Department of Mechanical Engineering, BM College of Technology, Indore (M.P.) India*

***Abstract*—This study investigates the predictive modelling of weld bead geometry in wire arc additive manufacturing (WAAM) through advanced machine learning methods. While WAAM is valued for its ability to produce large, complex metal parts with high deposition rates, precise control of the weld bead remains a critical challenge due to its influence on mechanical properties and dimensional accuracy. To address this problem, this study utilized machine learning approaches—Ridge regression, Lasso regression and Bayesian ridge regression, Random Forest and XGBoost—to predict the key weld bead characteristics, namely height, width and cross-sectional area. A Design of experiments (DOE) was used to systematically vary the welding current and travelling speed, with 3D weld bead geometries captured by laser scanning. Robust data pre-processing, including outlier detection and feature engineering, improved modelling accuracy. Among the models tested, XGBoost provided the highest prediction accuracy, emphasizing its potential for real-time control of WAAM processes. Overall, this study presents a comprehensive framework for predictive modelling and provides valuable insights for process optimization and the further development of intelligent manufacturing systems.**

***Index Terms*—wire arc additive manufacturing (WAAM); predictive modelling; machine learning; weld bead geometry; XGBoost.**

I. INTRODUCTION

Wire Arc Additive Manufacturing (WAAM) has emerged as a transformative approach within the broader spectrum of Additive Manufacturing (AM) technologies. By utilizing arc welding as the heat source and wire as the material input, WAAM enables the production of large, complex metal components with high deposition rates at low costs [1,2]. This unique approach differs from other AM processes such as Powder Bed Fusion (PBF) and Directed Energy Deposition (DED) as it enables the production of large-sized metal components, making it particularly relevant for industries such as aerospace, automotive, shipbuilding and heavy machinery production [3,4].

However, despite these promising advantages, WAAM has several process-related challenges that must be addressed to improve its industrial applicability. One of the most critical issues with this technology is the high heat input, which contributes to uneven thermal cycles and microstructural inconsistencies during layer-by-layer deposition [5]. This results in coarse and anisotropic grain structures, increasing residual stresses and reducing mechanical performance compared to other AM methods [6]. Additionally, rapid heating and cooling cycles can lead to porosity, cracking, and poor interlayer bonding, which further degrades component quality [7]. These defects are particularly pronounced in aluminum and titanium alloys, where oxidation and gas entrapment exacerbate microstructural weaknesses [5].

Beyond material-specific concerns, thermal distortions due to excessive heat input result in unwanted geometrical deviations, internal stresses, and part warping, which compromise dimensional accuracy [6]. The control of bead geometry, surface roughness, and defect formation also remains a major challenge [7,8], as these parameters significantly

influence the mechanical properties, surface finish, and post-processing requirements.

Accordingly, considerable efforts have focused on data-driven methods by integrating machine learning (ML) techniques [3,6,9]. Other areas include precise trajectory planning [10], integrating cooling conditions and material properties into trajectory design [11], employing thermal management to produce geometrically correct parts while reducing residual stresses [12–14] and, more recently, using artificial intelligence-based real-time multiparameter control has demonstrated significant potential for error-free manufacturing [15].

In addition to the areas mentioned, effective process monitoring underpins the production of high-quality WAAM components. Closed loop and real-time monitoring enable parameter adjustment that affect weld pool temperature and surface properties without compromising mechanical performance [16,17]. Thermal imaging cameras track temperature distribution, while laser scanners measure layer geometry and surface quality in real time [18]. Non-destructive evaluation methods—such as x-ray computed tomography (CT) and ultrasonic testing—help detect internal porosity and defects, ensuring part integrity [19,20]. High-speed cameras capture the dynamic behavior of the weld pool and metal transfer, offering insights into process stability [21,22]. Spectrometers, meanwhile, monitor the composition of deposited material, identifying any impurities or deviations from the target alloy [23].

Despite these advances, the control of weld bead geometry remains critically dependent on the fundamental process parameters of travel speed and current. In this study, the influence of variations in these parameters on bead geometry is therefore examined, with the aim of refining WAAM process models and ultimately improving final part quality.

Machine learning for WAAM

ML has proven invaluable for process optimization, quality control, and predictive modelling in WAAM. By predicting and controlling parameters such as electric current and travel speed, ML-based methods reduce trial-and-error iterations, enhance bead geometry, and minimize material waste [2,9]. Decision Trees, Random Forest, Support Vector Regression, Back Propagation Neural Networks, and XGBoost have all been employed to predict variables like surface roughness and defect formation [9,24]. Notably, XGBoost and artificial neural networks often deliver higher accuracy, especially with nonlinear input–output relationships [3,4]. In addition, advanced outlier detection techniques (e.g., local outlier factor) can help detect anomalies in welding data [25] while nested K-fold cross-validation reduces overfitting and yields robust performance estimates [26].

Parametric studies in WAAM

Parametric studies frequently focus on the influence of wire feed rate, travel speed, voltage, and interpass temperature across diverse welding materials and modelling methods. For instance, the authors of [27] employed a Taguchi test plan to optimize parameters affecting weld bead geometry and spatter, while in [28], wire feed rate and interpass temperature were investigated using an SVM-based weld bead modelling system. More complex parts were manufactured in [29] by systematically varying energy input, travel speed, and wire feed rate; however, further optimization and mechanical testing were deferred.

Study justification

Despite these advances, prior studies often address isolated aspects of WAAM modelling. This research provides a more comprehensive framework. The main aspects are presented in Table 1.

Table 1. Main aspects of study justification.

Aspect	Previous Studies	This Study
Data acquisition and cleaning	Focused on individual aspects of data collection and process modelling, often lacking systematic experimental design and advanced outlier detection [5,10,11,20]. Real-time monitoring limitations were highlighted [17]	Implements systematic Design of Experiments (DOE) and LOF-based outlier detection ([30]) for improved data robustness. Enhances real-time data acquisition for WAAM process monitoring
Feature extraction and dimensionality reduction	Relied on manual or basic feature extraction for bead geometry prediction	Automates 3D point cloud feature extraction and refines data for better

	with limited refinement [1,9,15,23]. AI-based process monitoring is emerging [18]	interpretability and model performance. Incorporates advanced feature engineering for defect prediction
Model validation	Conventional k-fold cross-validation used, but concerns remain regarding bias mitigation and generalization [3,9,12,24]	Employs nested k-fold cross-validation ([31]) to improve model generalization and selection robustness
Polynomial feature transformation	Nonlinear relationships in WAAM were noted but lacked systematic polynomial feature transformation [7,8,16,22]	Systematically explores polynomial transformations to capture nonlinear bead geometry variations
Model explainability	ML models were treated as "black boxes" with limited feature importance analysis [6,9,10,14,25]	Integrates SHAP analysis for feature contribution transparency, improving model interpretability
Model comparison	Previous studies compared ML models for WAAM outcomes but lacked a unified framework and ensemble methods [3,6,9,19,26,27]	Conducts a comprehensive ML model comparison, integrating ensemble and hybrid approaches for WAAM predictions

By uniting these methods, particularly FE, PF, rigorous validation, and model explainability, this study aims to establish a more holistic and reliable approach to ML-driven process modelling in WAAM.

II. MATERIALS AND METHODS

A three-stage process was employed to investigate the influence of welding parameters on the geometry of the resulting weld bead. This process included welding tests, measure- ment of weld seams, and computational analysis for extracting geometric properties. A summary of the process is presented in Figure 1.

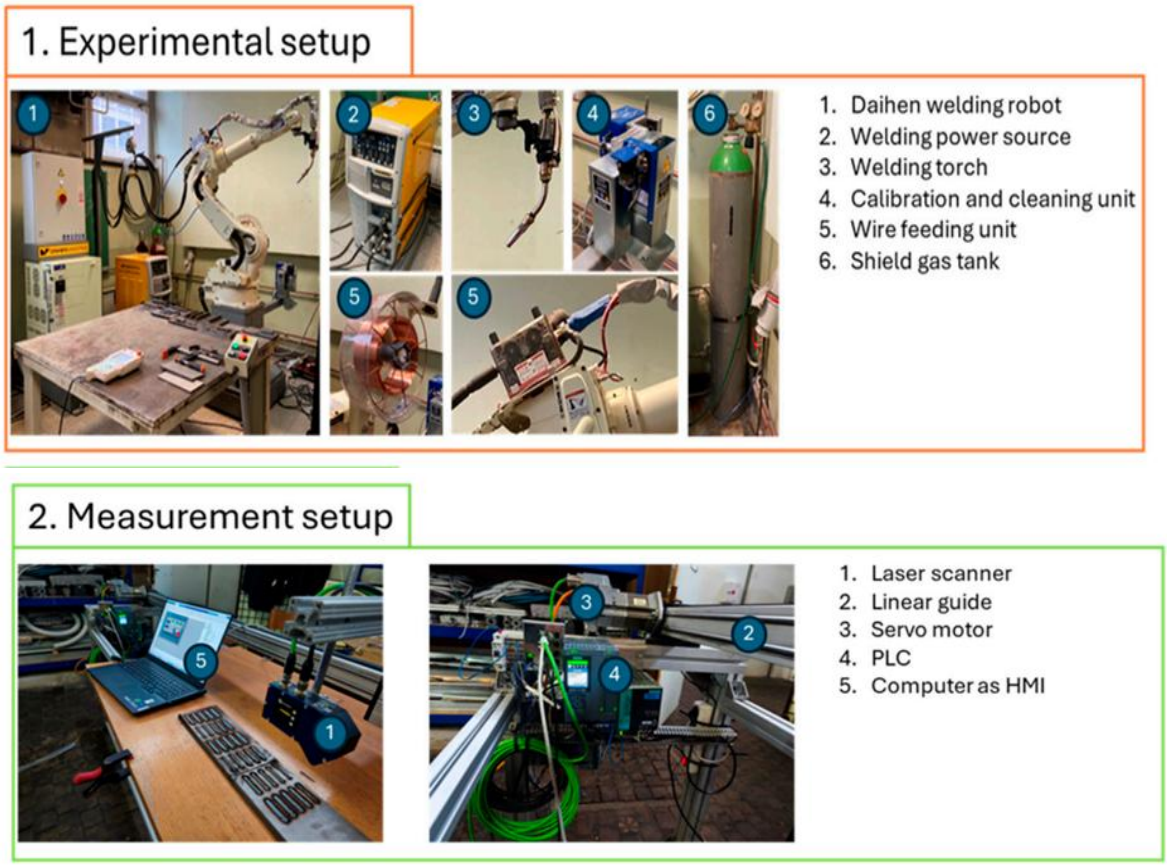

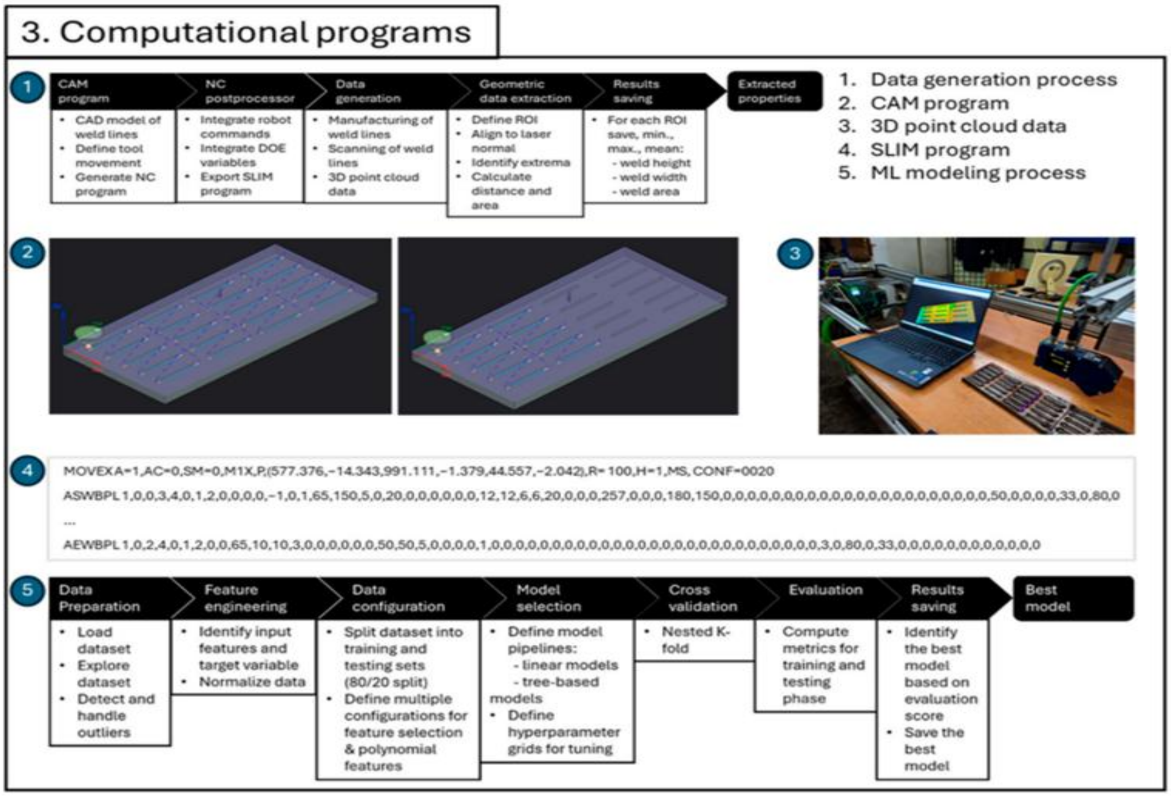

Figure 1. Materials and methods for modelling of weld bead geometry in wire arc additive manufacturing.

2.1 Experimental Setup

An experiment was conducted to examine how welding parameters influence the geometry of the resulting weld bead. The test utilized an S355 steel plate measuring 250 mm by 120 mm, along with a solid copper-coated welding wire (VAC 60) with a 1.2 mm diameter. The wire's chemical composition is presented in Table2.

Table 2. Chemical composition of VAC 60 welding wire.

Element	Weight Fraction [wt%]
C	0.08
Si	0.90
Mn	1.50
P	<0.025
S	<0.025

2.1.1. Robotic Cell

In the robotic cell, a Daihen NV8L-NEFC welding robot was paired with an FD1 controller. A WB-P500L DC welding power source was employed, and the robot was outfitted with an MTX group welding torch (featuring an integrated shock sensor), and a Daihen AF-4012 wire feeder. A mixture of argon and carbon dioxide was used as shielding gas. A J. Thielmann BRG-2000 DE served for calibration and cleaning. The robotic cell with all components was provided by Daihen Varstroj Slovenia.

Offline programming in SLIM (Standard Language for Industrial Manipulator) language which complies with the JIS B8439 standard was performed, requiring only three commands: MOVEX for motion and ASWBPL/AEWBPL for arc start/end. Robot motion control was restricted to movement type (linear or point-to-point), coordinates, speed, and configuration; welding current and travel speed were the adjustable parameters for the process.

2.1.2. Experimental Matrix

A full factorial design was applied with two independent variables (welding current and travel speed) and three dependent variables (bead height, width, and cross-section area). Welding current ranged from 65–155 A (in 10 A increments) and travel speed ranged from 20–40 cm/min (in 5 cm/min increments), resulting in 50 welded lines (testing samples). Arc

start/end parameters remained constant and "Synergic Mode" automatically adjusted voltage based on welding current. Table A1 presents experimental data together with the extracted features.

2.2. Measurement Setup

A Wenglor MLWL 132 laser scanner (Tettnang, Germany) was used to measure the weld bead surface. The sensor was mounted on a servo-driven linear guide for threedimensional scanning. A Siemens PLC S7-1500 (Munich, Germany) with an S120 CU310 controller (Munich, Germany) controlled the linear unit, and the scanning was initiated at 0.5 mm intervals. The measurement data was transmitted via TCP/IP to a computer running MATLAB R2023b, where it was stored in PLY format. The computer also served as a virtual human–machine interface (HMI).

2.3. Computational Programs

Several computer programs were developed to support the WAAM process and analyze the results. A CAM setup was modelled in Siemens NX, generating toolpaths and G-code for post-processing. A custom post-processor handled welding activation and welding and non-welding movements. Robot-specific commands were added, including work frame setup and tool cleaning. A custom algorithm extracted geometric properties from 3D scan data. Since the definition of the regions of interest for the extraction of the geometric features was done manually and based on the visual identification of the start and end zones of the weld bead arc, an outlier detection algorithm was integrated to identify possible poorly defined regions of interest. Different ML algorithms were trained on the prepared data to model geometric properties, and the best was chosen based on performance metrics.

2.3.1. CAM Programming

In Siemens NX, a base plate and 50 welding lines of 40 mm each were modelled to prepare the CAM setup for the welding process. The manufacturing coordinate system was defined in the plate's corner. The freeform_additive_fixed_axis_thinwall operation from the NX Additive Manufacturing add-on was used to generate the tool paths. Linear movements were specified for engagement, retraction, and transfer, with a 10 mm safety distance above the plate for transfers.

2.3.2. Postprocessor

NC code exported from Siemens NX was automated through the postprocessor, which converted motion commands into the required SLIM format and integrated DOE variables for welding. The NC code text file was loaded and analyzed, and the robot frame was aligned with the manufacturing coordinate system. Robot configuration and linear/pointto-point commands were adjusted to ensure desired speeds, and position/orientation coordinates were extracted with process-specific transformations applied. The DOE welding process was integrated by replacing deposition-activation commands with arc-start commands and adding experimental variables for robot travel speed and welding current. Safety and cleaning routines were added at the start of the program. Finally, a modified SLIM-format program was generated, ensuring the required structure and robot compatibility. ,

2.3.3. Algorithm for Extraction of Geometric Properties

An algorithm was developed to extract geometric properties from the line laser scanner data by processing 3D point clouds and isolating regions of interest (ROIs). ROIs were individually and manually defined for each weld bead by filtering data points on spatial coordinates. Because the plate and laser scanner were not aligned and the base plate was curved due to thermal stress, point cloud data had to be realigned with the sensor's XY plane. First, welded bead points were separated from base plate points. Next, a plane was fitted to the base plate, rotated to align with the XY sensor plane, and translated to the Z = 0 plane. A transformation matrix was created from these steps and applied to each point in the constrained ROI. After the transformation, geometric features (height, width and area) were extracted. For each scan line in the Y direction, height, width, and area were calculated using maximum/minimum X and Z values, and a polygon-based area calculation. Finally, minimum, average, and maximum values for each feature were calculated across the Y direction.

2.3.4. Data Analysis and Modelling Techniques

Once the geometric properties were extracted, data analysis and modelling techniques were used to transform the raw data into actionable insights. In the first phase, outliers were detected so that anomalies could be identified and corrected to ensure cleaner and more reliable datasets. The data were then standardized to ensure that feature scales were aligned

for improved model stability and performance. As the framework progressed, ML modelling techniques were implemented to create predictive models that capture relationships within the data. Regression metrics were used to evaluate the performance of the models created. This structured approach enabled comprehensive data analysis and predictive modelling. The employed ML modeling process is schematically shown in Figure 1.,

2.3.5. Data Standardization

To eliminate possible discrepancies in the size and units of the entered features, a normalization of the features was applied to the numerical data using z-score normalization. This technique transforms the data so that each feature has a mean of zero and a standard deviation of one [38]. This step prevents certain features from disproportionately influencing the model due to their larger size.

2.3.6. Nested K-Fold Cross-Validation for Model Improvement

The models were evaluated and the hyperparameters were tuned using nested kfold cross-validation to obtain an unbiased estimate of the model's generalization performance [31]. The nested cross-validation approach comprises two loops: an inner loop for optimizing the hyperparameters and an outer loop for evaluating the predictive ability of the model on unseen data. This prevents overfitting and allows for a more reliable evaluation of the model's performance on new data. Grid search cross validation was used to fine-tune the hyperparameters of the created models.

2.3.7. Regression Metrics for the Model Evaluation

The metrics used to evaluate the regression models created were R2 , mean absolute error (MAE), root mean square error (RMSE) and mean absolute percentage error (MAPE). Metric R2 provides a general indication of the predictive power, MAE reflects the closeness of the predictions to the actual values, RMSE is used to highlight larger errors, MAPE is used to assess the percentage error to provide a relative measure of accuracy. The variability of the prediction errors is indicated by the standard deviation of the residuals. These metrics were used to provide a comprehensive assessment of the accuracy, consistency and reliability of the model.

2.3.8. Addressing Potential Model Overfitting

Overfitting was mitigated through a comprehensive strategy that combined model regularization, hyperparameter tuning, and data preprocessing. Regularized linear models such as RR (using an L2 penalty) and LR (using an L1 penalty) inherently reduce model complexity by shrinking coefficients and eliminating irrelevant features, while BR leverages a Gaussian prior to naturally control coefficient sizes. In parallel, tree-based methods like RF and XGBoost were fine-tuned with constraints on parameters such as tree depth, the number of estimators, and regularization terms, further curbing the risk of overfitting. This approach was bolstered by a nested k-fold cross-validation framework that isolates hyperparameter optimization from model evaluation, ensuring unbiased estimates of predictive performance. Additionally, data standardization and outlier detection using the LOF contributed to a cleaner, more consistent dataset, preventing skewed model behavior due to noise or extreme values. These measures were undertaken not only to address potential pitfalls of overfitting but also to fully leverage the relatively small dataset, ensuring that its inherent quality and subtle patterns were effectively captured without succumbing to noise.

III. RESULTS AND DISCUSSION

3.1. Manufacturing and Geometric Properties Extraction

The weld beads produced are displayed in Figure 2, featuring three base plates, each divided into two scan areas. The welding sequence, determined experimentally, is indicated by numbers 1–50 and arrows.

Methodology

Milling experiments were conducted on AISI D2, D3 (cold work steels), H13 (hot work steel), and P20 (plastic injection mold steel) using coated and uncoated carbide tools. The cutting parameters—speed (75, 100, 125 m/min), feed (0.01, 0.015, 0.02 mm/tooth), and constant 0.5 mm depth of cut—were selected to evaluate performance under dry, wet (soluble oil flood coolant), and LN2 cryogenic cooling.

The developed cryogenic cooling system delivered LN2 using pressurized stainless steel pipes and nozzles precisely at the tool-chip interface. Cutting temperature was measured by a non-contact infrared pyrometer, cutting forces via a Kistler piezo-electric dynamometer, and surface roughness with a Taylor-

Hobson surface tester. Tool wear was observed under a microscope and scanning electron microscope to assess flank wear and morphological changes. Chip morphology was qualitatively analyzed by SEM imaging.

The experimental setup included the ARIX VMC 100 CNC vertical machining center. Each condition was replicated to ensure data reliability. Data acquisition software recorded force and temperature metrics. Experimental procedures followed IS standards for machining and safety. Results were statistically analyzed to evaluate the significance of cryogenic cooling effects

Results and Discussion

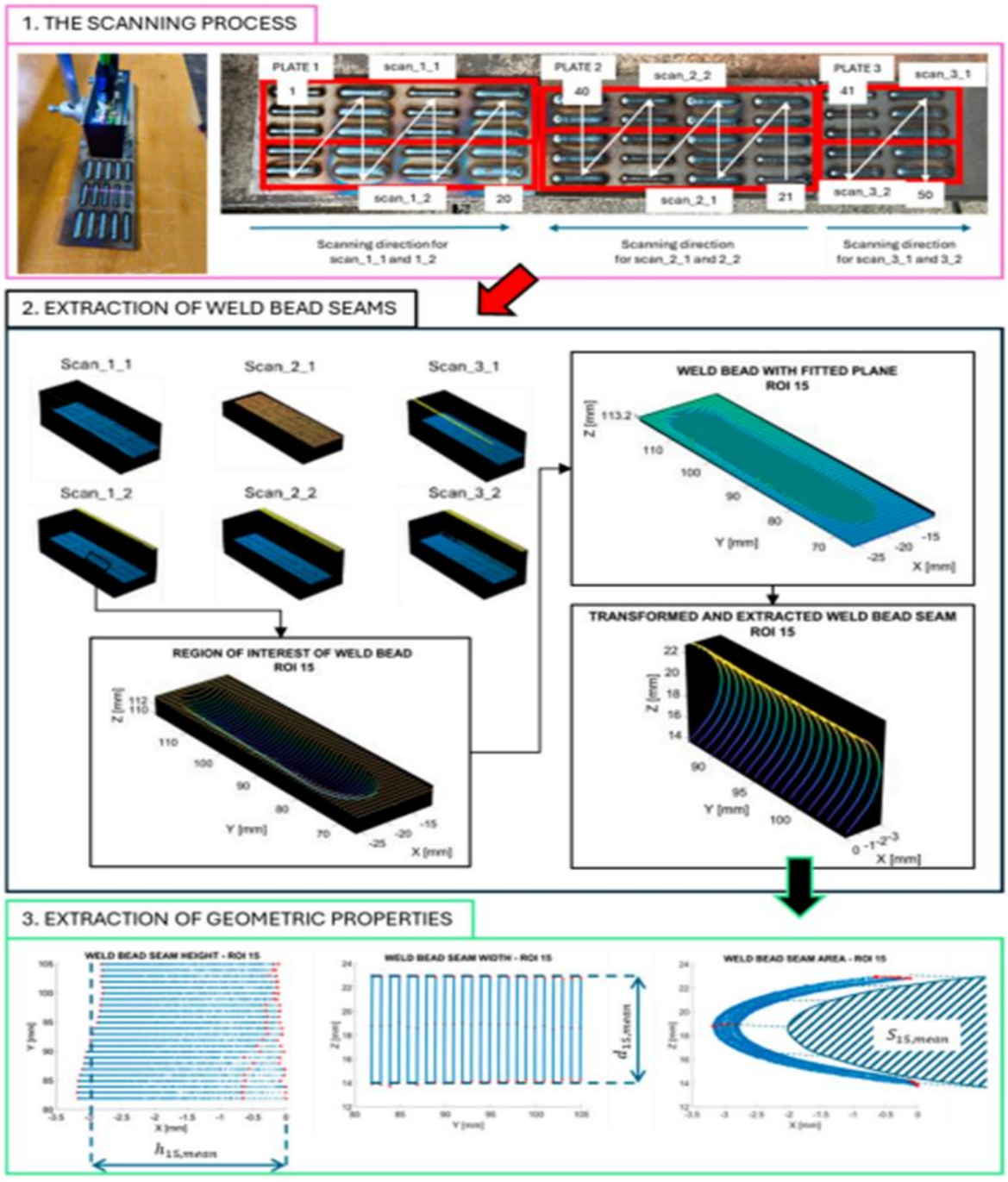

Each base plate is represented by two point clouds. Scan_1_1 and scan_1_2 represent the first base plate. When evaluating the geometric properties of the weld beads, each weld bead was extracted separately from the point cloud of the corresponding base plate by defining regions of interest (ROI). The extracted point clouds were then split into the points that represent the base plate and were used to align the scanned data to the scanner normal plane, and the points that represent the weld beads. The weld bead seams were determined by a narrower ROI that also excludes the arc start and end areas, which were not considered in this study, from the overall geometry of the weld bead.

Tool For each of the extracted weld bead seams nine features were computationally extracted: minimum, average and maximum weld height, width and area. For each scan line, the maximum point in the Z direction (red points in Figure 2) was used to determine the weld bead height. The maximum and minimum points in the X direction were used to calculate the weld bead width. The weld bead area was obtained by polygonizing all scan line points with respect to the Z axis. From these data, the minimum, average, and maximum weld height, width, and area of the entire weld bead seam were determined. The processed results are shown in Table A1, where the first column is the experiment number and the second and third columns are the independent parameters current and travel speed. The remaining columns are the minimum, average and maximum weld height, width and area.

3.2. Outlier Detection

The LOF settings used in the study—a configuration with 20 neighbors, a 5% contamination rate, and the Euclidean metric—represent a balanced approach to anomaly detection. However, since no outliers were detected, there are two possible interpretations: the dataset itself might be inherently robust, or the chosen settings may not be stringent enough to capture subtler anomalies. It is also important to consider that overly rigorous detection can be counterproductive; if the criteria are too strict, legitimate data points might be erroneously classified as outliers and removed, leading to a loss of valuable information and potentially harming the model's generalizability. Thus, while the current parameter settings may be adequate for certain anomalies, they might overlook less obvious ones, and overly strict detection could compromise model performance. Future work might benefit from further parameter tuning or incorporating complementary methods to ensure a more comprehensive detection of all anomalies.

IV. CONCLUSIONS

The XGBoost regression models augmented with feature engineering and polynomial transformations showed the strongest predictive performance for all three target variables— mean weld height, mean weld width and mean weld cross-section area. Mean weld height

The model achieved a training R2 of 0.980 and a test R2 of 0.868, indicating that it captured most of the variance and generalized well to unseen data. Contrary to feature importance analysis, the SHAP analysis revealed that current was the most influential parameter, exhibiting the broadest range of SHAP values, indicating its impact on the model's predictions. The SHAP dependence plot further illustrated a generally positive correlation between current and its impact on predictions, with variations in travel speed influencing this relationship. Additionally, the interaction term (current × travel speed) showed increased significance at higher travel speeds, suggesting a complex interplay between these factors in determining the output.

Mean weld cross-section area

The model achieved a training R2 of 0.999 and a test R2 of 0.931, demonstrating both remarkable precision and stability. Current was again the most important factor, accounting for 55.40% of the feature's importance, closely followed by travel speed at 39.41%. The SHAP analysis confirmed the dominant influence of current as it had the widest range of SHAP values.

These results emphasize the importance of current in predicting mean weld height, mean weld width and cross-section area. Although the interaction term between current and travel speed was less influential, it provided important insights into nonlinear and synergistic relationships. The low error metrics of the models (MAE, RMSE, MAPE) and the high Pearson correlation coefficients confirm their reliability. Supported by feature importance analyses and SHAP analyses, these results provide practical guidance for

the optimization of welding parameters to achieve precise control of welding results. Future work

It is planned that the study be expanded in future work by incorporating additional independent variables—namely, voltage, wire feed speed, shielding gas flow rate and composition, electrode/nozzle size, and arc length—and by evaluating key material properties such as tensile strength, toughness, fracture mechanics, microstructure, cracks, and porosity. Moreover, the modelling procedure is to be extended to multi-layer builds, with layer count introduced as a new variable, and investigations on stainless steel as well as combinations of plain and stainless steel to be conducted.

REFERENCES

[1] Kazmi, K.H.; Chandra, M.; Rajak, S.; Sharma, S.K.; Mandal, A.; Das, A.K. Implementing Machine Learning in Robotic Wire Arc Additive Manufacturing for Minimizing Surface Roughness. Int. J. Comput. Integr. Manuf. 2024, 38, 255–270. [CrossRef]

[2] Jatti, V.S.; Jatti, A.V.; Mishra, A.; Dhabale, R.D.; Sefene, E.M. Optimizing Flexural Strength of Fused Deposition Modelling Using Supervised Machine Learning Algorithms. Int. J. Inf. Technol. 2023, 15, 2759–2766. [CrossRef]

[3] Chandra, M.; Vimal, K.E.K.; Rajak, S. A Comparative Study of Machine Learning Algorithms in the Prediction of Bead Geometry in Wire-Arc Additive Manufacturing. Int. J. Interact. Des. Manuf. 2023, 18, 6625–6638. [CrossRef]

[4] Wu, Y.; Li, Z.; Wang, Y.; Guo, W.; Lu, B. Study on the Process Window in Wire Arc Additive Manufacturing of a High Relative Density Aluminum Alloy. Metals 2024, 14, 330. [CrossRef]

[5] Srivastava, M.; Rathee, S.; Tiwari, A.; Dongre, M. Wire Arc Additive Manufacturing of Metals: A Review on Processes, Materials and Their Behaviour. Mater. Chem. Phys. 2023, 294, 126988. [CrossRef]

[6] Pant, H.; Arora, A.; Gopakumar, G.S.; Chadha, U.; Saeidi, A.; Patterson, A.E. Applications of Wire Arc Additive Manufacturing (WAAM) for Aerospace Component Manufacturing. Int. J. Adv. Manuf. Technol. 2023, 127, 4995–5011. [CrossRef]

[7] Qu, G.; Guo, W.; Shi, J.; He, D.; Zhang, Y.; Dong, Y.; Chi, J.; Shen, Z.; Li, Y.; Chen, Z.; et al. Improvement of Gradient Microstructure and Properties of Wire-Arc Directed Energy Deposition Titanium Alloy via Laser Shock Peening. Mater. Sci. Eng. A 2024, 918, 147422. [CrossRef]

[8] Zhang, H.; Bai, X.; Dong, H.; Zhang, H. Modelling and Prediction of Process Parameters with Low Energy Consumption in Wire Arc Additive Manufacturing Based on Machine Learning. Metals 2024, 14, 567. [CrossRef]

[9] Denkena, B.; Wichmann, M.; Boß, V.; Malek, T. Technological Simulation of the Resulting Bead Geometry in the WAAM Process Using a Machine Learning Model. In Proceedings of the Procedia CIRP; Elsevier B.V.: Amsterdam, The Netherlands, 2024; Volume 126, pp. 627–632.

[10] Shah, A.; Aliyev, R.; Zeidler, H.; Krinke, S. A Review of the Recent Developments and Challenges in Wire Arc Additive Manufacturing (WAAM) Process. J. Manuf. Mater. Process. 2023, 7, 97. [CrossRef]

[11] Liu, J.; Xu, Y.; Ge, Y.; Hou, Z.; Chen, S. Wire and Arc Additive Manufacturing of Metal Components: A Review of Recent Research Developments. Int. J. Adv. Manuf. Technol. 2020, 111, 149–198. [CrossRef]

[12] Wu, Q.; Mukherjee, T.; De, A.; DebRoy, T. Residual Stresses in Wire-Arc Additive Manufacturing—Hierarchy of Influential Variables. Addit. Manuf. 2020, 35, 101355. [CrossRef]

[13] Liu, Y.; Shi, J.; Wang, Y. Evolution, Control, and Mitigation of Residual Stresses in Additively Manufactured Metallic Materials: A Review. Adv. Eng. Mater. 2023, 25, 2300489. [CrossRef]

[14] Srivastava, S.; Garg, R.K.; Sharma, V.S.; Sachdeva, A. Measurement and Mitigation of Residual Stress in Wire-Arc Additive Manufacturing: A Review of Macro-Scale Continuum Modelling Approach. Arch. Comput. Methods Eng. 2021, 28, 3491–3515. [CrossRef]

[15] Mattera, G.; Nele, L.; Paolella, D. Monitoring and Control the Wire Arc Additive Manufacturing Process Using Artificial Intelligence Techniques: A Review. J. Intell. Manuf. 2024, 35, 467–497. [CrossRef]

[16] Hölscher, L.V.; Hassel, T.; Maier, H.J. Development and Evaluation of a Closed-Loop z-Axis Control Strategy for Wire-and-ArcAdditive Manufacturing Using the Process Signal. Int. J. Adv. Manuf. Technol. 2023, 128, 1725–1739. [CrossRef]

[17] Franke, J.; Heinrich, F.; Reisch, R.T. Vision Based Process Monitoring in Wire Arc Additive Manufacturing (WAAM). J. Intell. Manuf. 2024. [CrossRef]

[18] Rahman, M.A.; Jamal, S.; Cruz, M.V.; Silwal, B.; Taheri, H. In Situ Process Monitoring of Multi-Layer Deposition in Wire Arc Additive Manufacturing (WAAM) Process with Acoustic Data Analysis and Machine Learning. Int. J. Adv. Manuf. Technol. 2024, 132, 5087–5101. [CrossRef]

[19] Derekar, K.Š.; Addison, A.; Joshi, S.S.; Zhang, X.; Lawrence, J.; Xu, L.; Melton, G.; Griffiths, D. Effect of Pulsed Metal Inert Gas (Pulsed-MIG) and Cold Metal Transfer (CMT) Techniques on Hydrogen Dissolution in Wire Arc Additive Manufacturing (WAAM) of Aluminium. Int. J. Adv. Manuf. Technol. 2020, 107, 311–331. [CrossRef]

[20] Treutler, K.; Wesling, V. The Current State of Research of Wire Arc Additive Manufacturing (WAAM): A Review. Appl. Sci. 2021, 11, 8619. [CrossRef]

[21] Halisch, C.; Radel, T.; Tyralla, D.; Seefeld, T. Measuring the Melt Pool Size in a Wire Arc Additive Manufacturing Process Using a High Dynamic Range Two-Colored Pyrometric Camera. Weld. World 2020, 64, 1349–1356. [CrossRef]

[22] Chen, T.; Xue, S.; Zhang, P.; Wang, B.; Zhai, P.; Long, W. Investigation on the Dynamic Behavior of Weld Pool and Weld Microstructure during DP-GMAW for Austenitic Stainless Steel. Metals 2020, 10, 754. [CrossRef]

[23] Alcaraz, J.Y.; Sharma, A.; Tjahjowidodo, T. Predicting Porosity in Wire Arc Additive Manufacturing (WAAM) Using Wavelet Scattering Networks and Sparse Principal Component Analysis. Weld. World 2024, 68, 843–853. [CrossRef]

[24] Barrionuevo, G.O.; Sequeira-Almeida, P.M.; Ríos, S.; Ramos-Grez, J.A.; Williams, S.W. A Machine Learning Approach for the Prediction of Melting Efficiency in Wire Arc Additive Manufacturing. Int. J. Adv. Manuf. Technol. 2022, 120, 3123–3133. [CrossRef]

[25] Transactions on Intelligent Welding Manufacturing; Chen, S., Zhang, Y., Feng, Z., Eds.; Springer: Singapore, 2019; ISBN 978-981-13- 8667-1.

[26] Cheepu, M. Machine Learning Approach for the Prediction of Defect Characteristics in Wire Arc Additive Manufacturing. Trans. Indian Inst. Met. 2023, 76, 447–455. [CrossRef]

[27] Wang, H.; Klaric, S.; Havrlišan, S. Preliminary Study of Bead-on-Plate Welding Bead Geometry for 316L Stainless Steel Using GMAW. FME Trans. 2024, 52, 563–572. [CrossRef]

[28] Ding, D.; Yuan, L.; Huang, R.; Jiang, Y.; Wang, X.; Pan, Z. Corner Path Optimization Strategy for Wire Arc Additive Manufacturing of Gap-Free Shapes. J. Manuf. Process. 2023, 85, 683–694. [CrossRef]

[29] Plangger, J.; Schabhüttl, P.; Vuherer, T.; Enzinger, N. CMT Additive Manufacturing of a High Strength Steel Alloy for Application in Crane Construction. Metals 2019, 9, 650. [CrossRef]

[30] Breunig, M.M.; Kriegel, H.-P.; Ng, R.T.; Sander, J. LOF. ACM SIGMOD Record 2000, 29, 93–104. [CrossRef]

[31] Abdulaal, M.J.; Casson, A.J.; Gaydecki, P. Performance of Nested vs. Non-Nested SVM Cross-Validation Methods in Visual BCI: Validation Study. In Proceedings of the 2018 26th European Signal Processing Conference (EUSIPCO), Roma, Italy, 3–7 September 2018; IEEE: Piscataway, NJ, USA, 2018; pp. 1680–1684.

[32] Hoerl, A.E.; Kennard, R.W. Ridge Regression: Biased Estimation for Nonorthogonal Problems. Technometrics 2000, 42, 80–86. [CrossRef]

[33] Tibshirani, R. Regression Shrinkage and Selection via the Lasso. J. R. Stat. Soc. Ser. B 1996, 58, 267–288. [CrossRef]

[34] MacKay, D.J.C. Bayesian Interpolation. Neural Comput. 1992, 4, 415–447. [CrossRef]

[35] Breiman, L. Random Forests. Mach. Learn. 2001, 45, 5–32. [CrossRef]

[36] Chen, T.; Guestrin, C. XGBoost: A Scalable Tree Boosting System. In Proceedings of the ACM SIGKDD International Conference on

Knowledge Discovery and Data Mining, San Francisco, CA, USA, 13–17 August 2016; Association for Computing Machinery: New York, NY, USA, 2016; pp. 785–794.

[37] Singh, K.; Upadhyaya, S. Outlier detection: Applications and techniques. Int. J. Comput. Sci. Issues (IJCSI) 2012, 9, 307.

[38] Cheadle, C.; Vawter, M.P.; Freed, W.J.; Becker, K.G. Analysis of Microarray Data Using Z Score Transformation. J. Mol. Diagn. 2003, 5, 73–81. [CrossRef]